


Article

# Research on the Randomness of Low-Voltage AC Series Arc Faults Based on the Improved Cassie Model

Yao Wang <sup>1</sup> , Yuying Liu <sup>1</sup>, Xin Ning <sup>2,3,\*</sup>, Dejie Sheng <sup>1</sup> and Tianle Lan <sup>1</sup>

<sup>1</sup> State Key Laboratory of Reliability and Intelligence of Electrical Equipment, Hebei University of Technology, Tianjin 300400, China; wangyao@hebut.edu.cn (Y.W.); liuyuying2022@stu.hebut.edu.cn (Y.L.); shengdejie2023@stu.hebut.edu.cn (D.S.); lantianle2023@stu.hebut.edu.cn (T.L.)

<sup>2</sup> Power Internet of Things Key Laboratory of Sichuan Province, Chengdu 610041, China

<sup>3</sup> State Grid Sichuan Electric Power Research Institute, Chengdu 610041, China

\* Correspondence: x.ning@stu.xjtu.edu.cn

**Abstract:** Low-voltage AC power lines are prone to arc faults, and an arc current presents as a random and complicated signal. The amplitude of the line current remains relatively unchanged during the occurrence of series arcs, hence complicating the detection of series arc faults. In this work, we developed a low-voltage series arc fault test platform to analyze the digital features of low-voltage series arc currents and the morphology of arc combustion, as the current model fails to capture the high-frequency and randomness of arc currents. An analysis of the physical causes and influencing factors of the random distribution of AC arc zero-crossing times was conducted. A time-domain simulation model for arc fault currents was developed by enhancing the time constant of the Cassie arc model, while the high-frequency features of arc currents were simulated using a segmented noise model. The measured arc current data were utilized to validate the model through the analysis of the zero-crossing time distribution of arc current, the correlation coefficient of the arc current frequency-domain signal, and the similarity of the time-domain waveforms. When comparing the similarity of the simulated waveforms of the arc model presented in this research and those of other traditional arc models, it was found that the suggested model effectively characterizes the time-/frequency-domain features of low-voltage AC series arc fault currents. The suggested model enhances the features of randomness in low-voltage AC series arc faults and is important in extracting essential aspects and reliably recognizing low-voltage series arc faults.

**Keywords:** low-voltage arc fault; series arc; arc model; randomness; zero-crossing time



Academic Editor: King Jet Tseng

Received: 30 December 2024

Revised: 17 January 2025

Accepted: 20 January 2025

Published: 24 January 2025

**Citation:** Wang, Y.; Liu, Y.; Ning, X.; Sheng, D.; Lan, T. Research on the Randomness of Low-Voltage AC Series Arc Faults Based on the Improved Cassie Model. *Energies* **2025**, *18*, 538. <https://doi.org/10.3390/en18030538>

**Copyright:** © 2025 by the authors. Licensee MDPI, Basel, Switzerland. This article is an open access article distributed under the terms and conditions of the Creative Commons Attribution (CC BY) license (<https://creativecommons.org/licenses/by/4.0/>).

## 1. Introduction

According to official figures from the Fire and Rescue Bureau of the Ministry of Emergency Management, between January and August 2024, China reported a total of 660,000 fires, with 31.4% attributed to electrical faults, marking them as the primary cause of these incidents [1]. Rising power usage is correlated with a yearly increase in electrical fire incidents resulting from equipment malfunctions and the aging of electrical lines. The low-voltage distribution network is an essential energy delivery infrastructure in contemporary life. Its structural complexity has resulted in numerous safety concerns and faults. The series arc fault, a prevalent fault type, poses significant hurdles to the safe operation of low-voltage distribution networks due to its detection and precise localization difficulties [1–3]. The electrical fire issue resulting from series arc faults, characterized by subtle fault traits, concealment, and randomness, is susceptible to the effects of power electronic nonlinear

loads, posing significant challenges to arc fault detection. Consequently, the associated fire risk warrants considerable attention [4]. In recent years, arc fault protectors and similar products have emerged on the market for the detection of arc faults. Nevertheless, the recognition accuracy of these devices is suboptimal, they are prone to malfunctions, and they lack extensive practical application testing [5]. The response time of low-voltage solid-state circuit breakers is approximately in the microsecond range, exceeding the operational speed of typical mechanical circuit breakers by almost 1000 times. They may respond swiftly when an arc fault transpires. However, in low-voltage conditions, solid-state circuit breakers experience significant current loss, resulting in energy loss and excessive heating. Power electronic devices in solid-state circuit breakers exhibit low withstand voltage, and the cutoff current is constrained in the off state [6,7]. Consequently, examining the randomness of low-voltage AC arc evolution and developing a current data model that precisely and thoroughly represents arc features is highly significant for research on arc fault location and detection.

Scholars have recently undertaken studies on the randomness of arc faults and modeling methods. In Reference [8], the authors employed a three-parameter Mayr model to simulate the zero-crossing features of an arc current; however, they posited that these features were invariant and failed to capture the inherent randomness of the arc. A two-dimensional axisymmetric-nozzle arc model based on magnetohydrodynamics was developed in [9], and a nozzle arc for air, SF<sub>6</sub>, and C<sub>4</sub>F<sub>7</sub>N/CO<sub>2</sub> mixed gas was computed. Using unified one-dimensional simulation, the mechanism of an AC arc in an argon-cooled electrode at atmospheric pressure was examined in [10]. A simplified equivalent heat-source model was proposed in [11] to substitute the magnetohydrodynamic model. In Reference [12], the authors enhanced the traditional black-box model by accounting for the variation in arc diameter at the zero-crossing point of the arc voltage, thereby providing a more precise depiction of the zero-crossing features of the arc voltage. While the aforementioned model elucidates the dynamic growth of an arc from its physical origins, it fails to capture the stochastic and high-frequency properties of arcs. In Reference [13], the authors delineated expressions for the time constant and dissipation power of the Mayr arc model as functions of arc conductance, with the parameters in the expression adjusted by a genetic algorithm. Nevertheless, the model is exclusively tuned to a particular arc-current waveform, making it challenging to represent the overarching principles of arc randomness. Using a neural network to adjust the parameters of the expanded Schavemaker arc model, extra samples with arc features were generated. In Reference [14], the authors studied the AC arc modeling technique using the simplified Schavemaker model. However, the arc's high-frequency features and randomness are not captured by the model. In order to examine the variations in combustion-time features of the secondary arc, the authors of Reference [15] used the chain-arc model's random model of the beginning position to simulate the secondary arc. An enhanced arc model was introduced in [16] that incorporated a time-varying random coefficient to depict the timing of arc extinction and reignition, building upon the original Mayr model. It can consistently replicate the randomness and intermittency of arc faults during the 'unstable arc period'. In Reference [17], the authors employed the enhanced Mayr arc model with other conventional arc mathematical models to calculate the rapid transient overvoltage waveform resulting from the closure of a UHV GIS disconnecter to a no-load short bus. Although the three studies mentioned above all modeled high-voltage arcs and captured their unpredictability to a certain extent, it is difficult to generalize the features of high-voltage arcs to low-voltage series arcs, since the randomness is assumed to exist at a certain level. In Reference [18], the authors established a low-voltage single-phase AC series arc fault experimental platform to investigate the strong randomness of series arc faults but did not detail their underlying causes. The three main kinds of oscillating

intermittent arcs were described in [19]: steady-state, semi-steady-state, and oscillating intermittent arc defects inside the cable. However, the features of continuous combustion's steady-state low-voltage AC arc faults cannot be adequately described by the previously proposed model. In Reference [20], the authors analyzed the high-frequency features of arcs under aviation conditions, enhancing the classical black box model through the examination of its voltage features, resulting in favorable outcomes. Nonetheless, low-voltage AC arcs lack these features and are inapplicable to the aforementioned model. In conclusion, current studies fail to quantitatively and accurately depict the stochastic properties of arc fault currents, and existing arc models do not concurrently represent both low-frequency and high-frequency features.

This article focused on low-voltage AC arc faults as the subject of study. A time-domain simulation model for arc fault current was developed with the enhanced Cassie arc model time constant, and a piecewise noise model was used to replicate the high-frequency features of arc current. The Pearson correlation coefficient between the arc current data from the suggested model simulation and the measured arc current data was employed to validate the model. The primary research focus of this work was as follows:

- (1) A test platform for series arc faults was established to acquire data on arc voltage, current, and the combustion morphological features of various electrical loads.
- (2) The mechanism of alternating current arcs was examined. An analysis of the random distribution of arc current zero-crossing time across various current levels was conducted. The mathematical expression for the zero-crossing time of an arc current was derived. The impact of the Cassie model's time constant on the zero-crossing time of an arc current was examined. A time-domain simulation model for arc current was constructed.
- (3) The arc current was divided based on the amplitude's frequency-dependent features, and a segmented noise model was introduced to simulate the high-frequency features of the arc current. The parameters were derived using a genetic algorithm. The enhanced Cassie model was integrated with the piecewise noise model through small signal analysis, and the Pearson correlation coefficient between the arc current data from the proposed model simulation and the measured arc current data was employed to validate the model under both linear and nonlinear loads. The findings indicate that the correlation between the simulated arc current waveform and the measured waveform is 99.16% for linear loads and 99.03% for nonlinear loads.

## 2. Data Collection and Analysis

### 2.1. Series Arc Fault Experimental Platform

A series arc fault test platform was constructed in accordance with the IEC 62606 standard [21], shown in Figure 1. The platform can replicate series arcs resulting from inadequate contact and deteriorating insulation under various operational settings. The testing platform comprises a 220 V/50 Hz AC power supply, a load branch, a data acquisition component, an arc generator, and additional elements. The arc generator can produce two types of arcs: point contact and carbonization path. To comprehensively understand the phenomenon of arc randomness, arc current and voltage were measured using current sensors and voltage measuring devices, while the Phantom V611 high-speed camera was employed to examine and document the arc topography features during arcing. The Phantom V611 high-speed camera (AMETEK® Group, Edison, NJ, USA) supports a resolution of  $1280 \times 800$  and a shooting rate of 30,000 frames per second, fulfilling the experimental criteria for real-time capture of arc discharge dynamics. Figure 2 shows the real test platform photo.

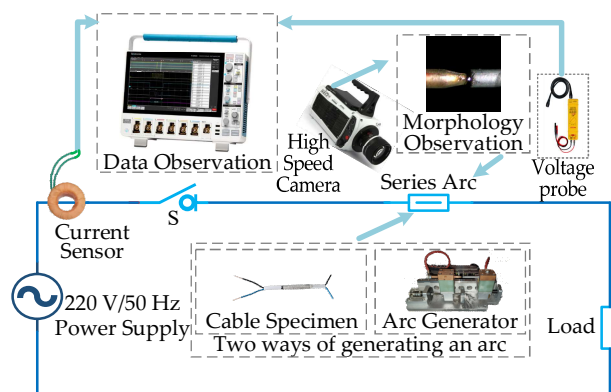


Figure 1. Series arc fault experimental platform.

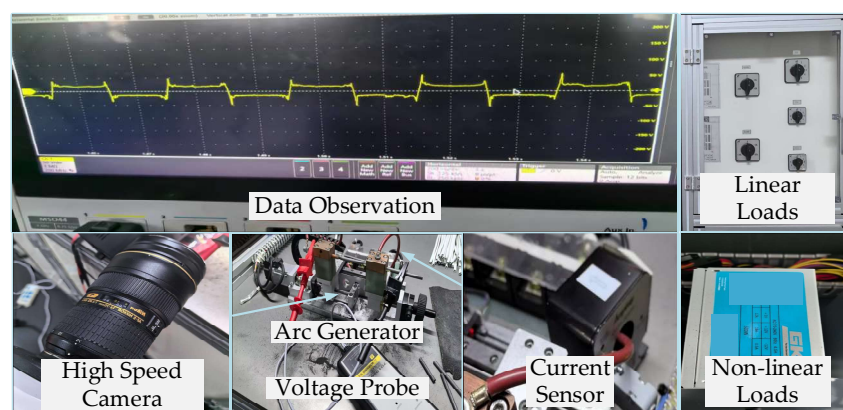


Figure 2. Real test platform photo.

According to IEC 62606 standards, the arc current data of 2.5 A, 5 A, 10 A, 16 A, and 32 A levels were collected within 150 s. In order to understand the features of higher-frequency arc currents, the sampling rate was set at 100 kHz. Furthermore, we chose linear and nonlinear loads as the experimental loads. The detailed information of the some devices is shown in Table 1.

Table 1. The detailed information of the some devices.

Name	Information
Power Supply	220 V/50 Hz, maximum current flow capacity 32 A
Voltage Probe	Bandwidth 200 MHz, attenuation ratio 1/100
Current Sensor	Bandwidth 800 kHz, attenuation ratio 500:1
High-Speed Camera	Maximum speed 65,000 fps, 1280 × 800
Linear Loads	5–80 Ω
Nonlinear Loads	Switch Mode Power Supply, 12 V/32 A, 700 W

## 2.2. Analysis of Arc Fault Current Features

In recent years, researchers both domestically and internationally have conducted extensive investigations on the features of arc fault electrical parameters, primarily focusing on the quantitative relationships among arc fault voltage, current, and energy, as well as their temporal variations [8,9,22,23]. The proliferation of nonlinear loads within the distribution network has resulted in increasingly intricate current waveform features. Consequently, the load’s normal current exhibits elevated harmonics and distortion, resembling an arc fault current, rendering traditional arc models inadequate for accurately representing arc fault features. Consequently, it is essential to examine the electrical properties of arcs within the distribution network context in both the time and frequency domains.

Initially, the time-domain data of the voltage and loop current between the electrodes in both arc and non-arc modes are acquired, as illustrated in Figure 3, leading to the following conclusions:

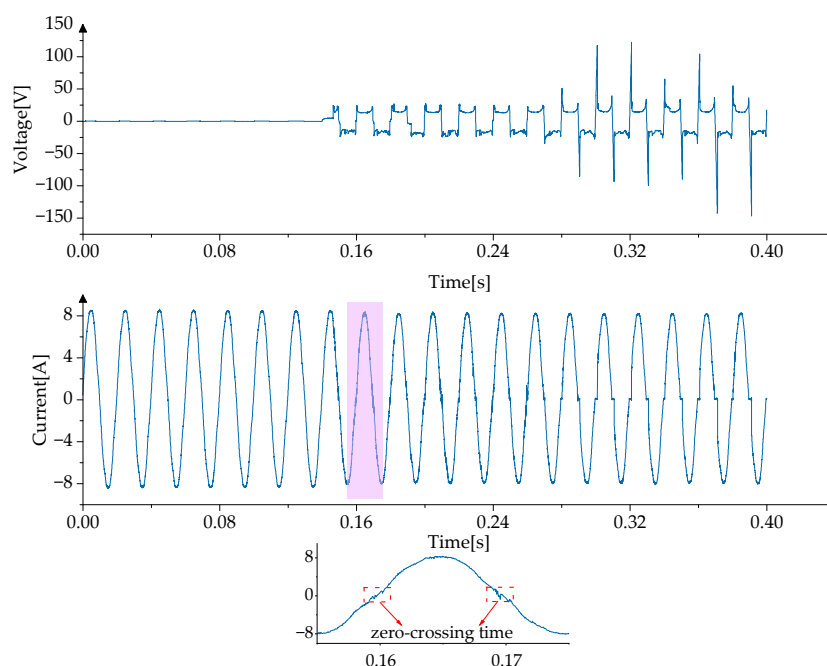


**Figure 3.** Waveforms of the voltage between the electrodes and the circuit current during arc development.

(1) During an arc fault, the electrode voltage abruptly rises from zero, resulting in peaks of arc ignition and extinction, with the intensity of arc burning markedly increasing as the combustion intensifies. The arc voltage will decrease to a certain value after first attaining the arc voltage until the current approaches zero, due to the medium's recovery between the electrodes, resulting in the arc voltage increasing to the arc extinguishing voltage.

(2) When an arc fault occurs, the line current exhibits the features of a flat shoulder (zero-crossing). AC line arcs are readily extinguished near the current zero-crossing; however, as the electrode voltage increases, the dielectric recovery strength of the air between the electrodes fails to match the voltage recovery intensity, leading to the re-ignition of the arc and affecting the zero-crossing features of the current.

(3) In the occurrence of an arc fault, the magnitude of the line current will be marginally diminished. When a series arc faults occurs in the circuit, the line behaves as a variable resistor, leading to an increased line resistance compared to the usual resistance, hence reducing the line current.

To accurately represent the trend of low-frequency components and the distribution of high-frequency components in arc fault currents, it is essential to differentiate between low-frequency and high-frequency bands, as indicated by the preceding analysis of time-domain features. Consequently, the discrete Fourier transform was applied to the arc current, segmenting it into equal-length time windows, and the arc fault current signal in the frequency domain was discretized and analyzed. The equation for the discrete Fourier transform is as follows:

$$X(k) = \sum_{n=0}^{N-1} x(n)e^{-j\frac{2\pi}{N}kn}, k \in [0, N-1] \quad (1)$$

where  $X(k)$  is the  $k$ -th component in the frequency domain of the signal,  $x(n)$  is the  $n$ -th sampling point in the time domain,  $N$  is the total number of sampling points, and  $j$  is the imaginary number unit. The time window was selected to be 20 ms, and the arc fault current spectrum was obtained by performing a fast Fourier transform on the low-voltage arc fault current, as shown in Figure 4. The sample rate to generate the arc fault current spectrum is 100 kHz.

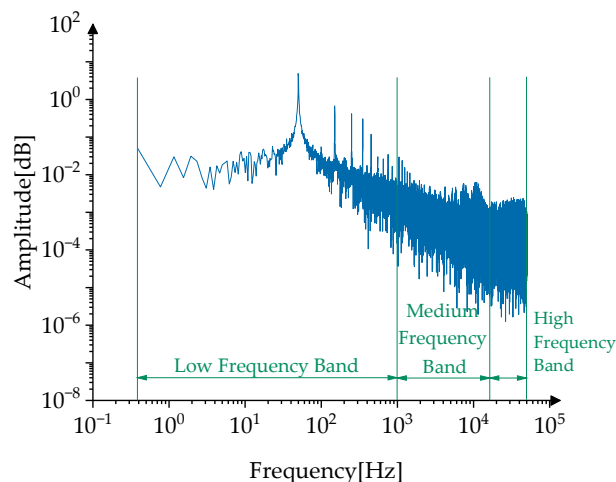


**Figure 4.** The spectrum of the arc fault current.

From the spectrum, it can be concluded that according to the law of spectral amplitude with frequency, the arc fault current can be divided into three frequency bands: a low-frequency band, a medium-frequency band, and a high-frequency band. Among them, the low-frequency band is mainly superimposed with the 50 Hz fundamental frequency AC signal and the 50 Hz integer frequency-doubling odd harmonic signal, which is the arc current feature before 1 kHz. In the frequency band above 1 kHz, the frequency-domain features of arc current can be divided into two stages: In the first stage, the amplitude of the arc fault current decreases with the increase in frequency, which is defined as the medium-frequency band, and in the second stage, the amplitude of the arc fault current basically does not change with the frequency and is stable in a small range, which is defined as a high-frequency band.

### 3. Analysis of Arc Fault Features and Influencing Factors

#### 3.1. Analysis of the Physical Features of Arcs

During the arc discharge process, electrons can be liberated from the electrode surface through heat emission, electric field emission, or light emission. The arc frequently occurs with significant arc phenomena, and the radiation from the arc causes the metal electrode surface to emit particles [24]. The interaction and energy exchange among particles influences the local electric field, resulting in its distortion. The time-varying external electric field causes localized alterations in the electric field of the electrode gap, resulting in the time-varying conductivity of the charged particles. Furthermore, the distribution of free electrons between the electrodes is stochastic, and the aggregation of free electrons fluctuates randomly, resulting in variations in the arc diameter [12]. The macroscopic phenomena indicate that the arc's impedance is locally discontinuous, impacting the current in the series circuit and the voltage across the electrode terminals, resulting in waveform jitter, burrs, and increased harmonic amplitude [16].

When an arc fault occurs, the voltage and current in the line have the following relationship:

$$V_m \sin(\omega t + \varphi) = i \left( \frac{1}{g} + r_0 \right) \quad (2)$$

In the equation,  $V_m$  is the peak voltage of the AC power supply,  $\varphi$  is the phase corresponding to the time of arc occurrence,  $i$  is the loop current,  $g$  is the admittance of the arc,  $r_0$  is the initial resistance of the line,  $\omega$  is the frequency of the AC power supply, and  $t$  is the time when the arc occurs. At the breakdown moment (defined as  $t = 0$ ), the breakdown voltage is as follows:

$$V_b = V_m \sin \varphi \quad (3)$$

The phase is  $\varphi$  at this time. When the phase angle is  $\pi$ , the current crosses zero, the arc goes out, and the current is turned on in the phase range of  $\varphi \sim \pi$ . The phase of the breakdown voltage can be derived from (2).

$$\varphi = \sin^{-1} \left( \frac{u}{V_m} (1 + gr_0) \right) \quad (4)$$

where  $u$  is the arc voltage corresponding to that moment. The on-time is obtained from (4).

$$\Delta t = \frac{\pi - \varphi}{\omega} = \frac{\pi - \sin^{-1} \left( \frac{u}{V_m} (1 + gr_0) \right)}{\omega} \quad (5)$$

The zero-crossing time of each half-cycle of the arc:

$$t_0 = \frac{T}{2} - \Delta t \quad (6)$$

That is, the zero-crossing time  $t_0$  of each half-cycle of the arc is related to the phase angle  $\varphi$  corresponding to the breakdown voltage.

### 3.2. Analysis of Random Features of Arcs

The AC current has a zero-crossing characteristic. When the arc burns, the thermal emission degree at the zero-crossing point of the current will be reduced, and the arc voltage of the resistive load will also be reduced, resulting in a decrease in the field emission electrons, so the AC arc current will be impacted by zero-crossing phenomenon [25]. The zero-crossing time is positively correlated with the arc voltage. When the electrode spacing is constant, the arc voltage changes randomly due to the local electric field change caused by electron collision formed by the field emission between the arcs. The change in the diameter of the arc and the conductivity of the particles in the electrode gap will cause a random change in the zero-crossing time of the arc current [12,25]. Therefore, the random change of the zero-crossing time reflects the randomness of the arc voltage.

According to IEC 62606 standards, the arc current data of 2.5 A, 5 A, 10 A, 16 A, and 32 A levels were collected. It can be seen from Figure 3 that the arc voltage and current have distortion phenomena such as peak fluctuation, burr, and flat shoulder. The window size is 20 ms. In order to cover the high-frequency band of the arc current, the sampling rate was set to 100 kHz, so the number of points in each time window was 2000. In order to avoid contingency, 500 windows were selected for each current level to analyze the statistical features of the zero-crossing time of the AC arc.

This study examined the probability distribution of arc zero-crossing time by computing the zero-crossing time of the arc current within a specified time interval during a single cycle. It employed log-normal, normal, and Weibull distribution functions to model the probability density of arc zero-crossing time. Table 2 and Figure 5 illustrate the fitting efficacy of the three aforementioned probability density functions for arc zero-crossing

duration at the 5 A current level. To facilitate a clearer comparison of the fitting efficacy of various probability density functions regarding the zero-crossing duration of the arc current, the Kolmogorov–Smirnov (K-S) test was employed to evaluate the goodness of fit of these probability density functions. A greater  $p$ -value indicates that the data distribution closely resembles the probability density function distribution. If  $p < 0.05$ , the data are deemed incompatible with the distribution. Table 2 indicates that the  $p$ -value for the log-normal distribution at the 5 A current level is the highest and substantially exceeds the  $p$ -values of the other two distributions. Upon analyzing a substantial dataset of arc current zero-crossing duration across all current levels, the  $p$ -value for the log-normal distribution consistently exhibited the highest value in all instances. Consequently, it could be inferred that the arc current zero-crossing time adheres to a log-normal distribution.

**Table 2.** Comparison of the fitting effects of different probability density functions.

Probability Density Function	Parameter	Parameter Estimation Value	Parameter Standard Deviation	$p$
Normal distribution	$\mu$	0.00456	0.00025	0.30685
	$\sigma$	0.00152	0.00018	
Log-normal distribution	$\mu$	−5.4402	0.05152	0.90133
	$\sigma$	0.31762	0.03717	
Weibull distribution	$\mu$	0.0051	0.00025	0.02444
	$\sigma$	3.20273	0.38431	

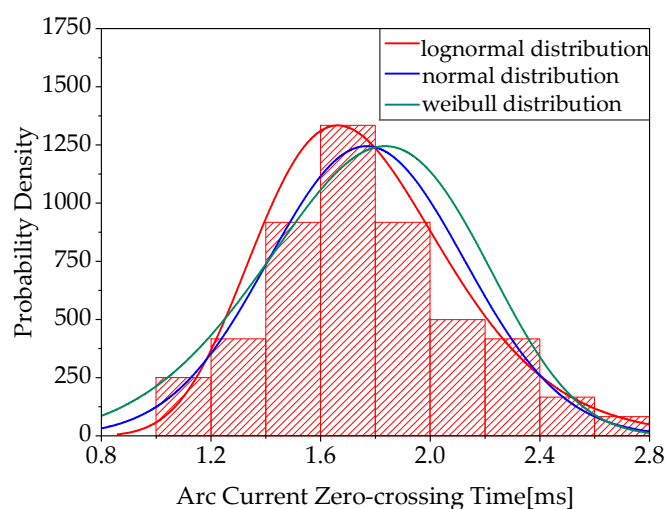


**Figure 5.** The arc current zero-crossing time distribution of the 5 A arc current.

The probability density distribution of arc current zero-crossing time under different current levels is shown in Figure 6. In the results shown in Figure 6, with the increase in current level, the peak value of the probability density of arc current zero-crossing time gradually moves to the left. Since the recovery strength of the arc gap medium is negatively correlated with the line current, the increase in the current level will reduce the recovery strength of the arc gap medium, which is conducive to the reignition of the arc, that is, the zero-crossing time of the arc current decreases and the overall distribution shifts to the left. Table 3 shows the optimal fitting parameters of the log-normal distribution of arc current zero-crossing time under different current levels.



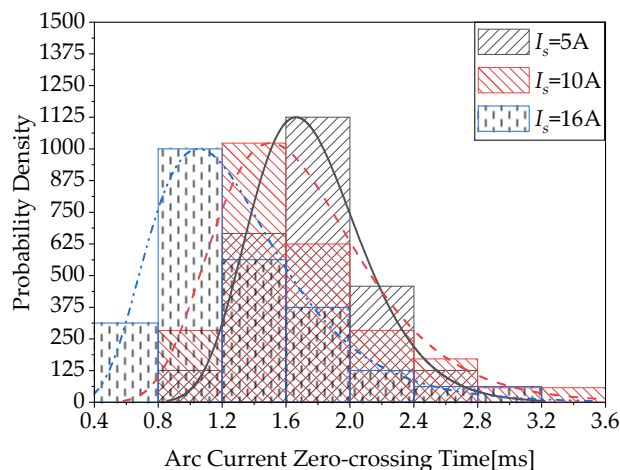


**Figure 6.** The arc current zero-crossing time distribution of different arc currents.

**Table 3.** Fitting parameter values for the arc current zero-crossing time distribution of different arc currents.

Current (A)	Parameter $\mu$ Estimation Value	Parameter $\sigma$ Estimation Value
2.5	−5.43859	0.24799
5	−5.4902	0.31762
10	−5.81361	0.51006
16	−5.89254	0.57203
32	−5.91376	0.61183

### 3.3. Analysis of Factors Influencing Zero-Crossing Time

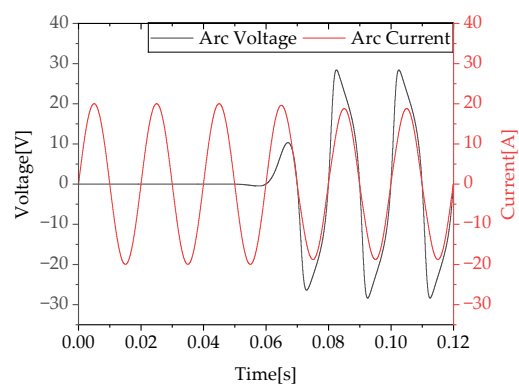
The classical arc models include the Cassie arc model and the Mayr model. The Cassie model considers that the arc temperature is evenly distributed and is suitable for scenes with low arc impedance at high current levels. In this paper, the zero-crossing time distribution features of series arc stable combustion in low-voltage distribution networks were studied, and the improved Cassie model was selected for arc simulation.

The expression of the Cassie model is as follows:

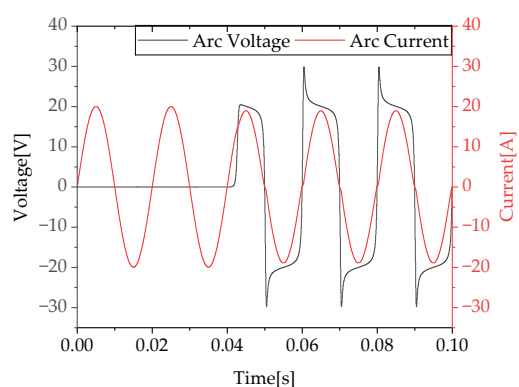
$$\frac{1}{g} \frac{dg}{dt} = \frac{1}{\tau} \left( \frac{u^2}{u_c^2} - 1 \right) \tag{7}$$

In (7),  $g$  is the admittance of the arc,  $\tau$  is the arc time constant, and  $u_c$  is the static voltage of the arc, which is also a constant.

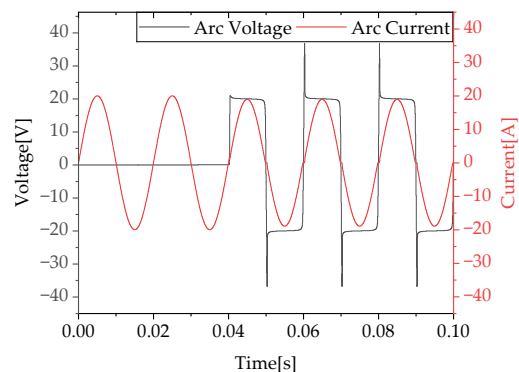
The time constant  $\tau$  of the arc affects the time required for the arc voltage to drop from the arcing peak voltage to a stable arc voltage value. When it is set to 0.04 s, the arc occurs, the arc static voltage  $u_c$  is set to 20 V, and the arc current and voltage changes with the change in time constant  $\tau$  are shown in Figure 7. It can be seen from Figure 7 that as the time constant  $\tau$  decreases, the time when the arc voltage drops from the arc peak to the stable value decreases, and the tilt degree at the zero-crossing point of the arc current is smaller, so the arc current zero-crossing time is longer. Due to the thermal inertia of the arc, the time constant  $\tau$  reflects that when the current changes rapidly, the air gap dissociation effect is too late to change, so the change of the arc conductance tends to be slow and the change speed of the arc voltage slows down, which not only affects the speed when the arc voltage drops from the arc peak to the stable value but also affects the rising speed of the arc voltage in the initial period of arcing. Therefore, when the time constant  $\tau$  is too large, as shown in Figure 7a, the arc voltage does not rise to the arc voltage value at 0.04 s.



(a)



(b)



(c)

**Figure 7.** The arc voltage and current curves when  $\tau$  changes. (a)  $\tau = 3 \times 10^{-3}$  s; (b)  $\tau = 3 \times 10^{-4}$  s; (c)  $\tau = 3 \times 10^{-5}$  s.

The arc static voltage  $u_c$  reflects the size of the arc voltage. The peak value of the IEC standard static recovery voltage is taken. When the arc current passes zero in the AC arc, if the arc gap resistance is considered to be infinite, the transient recovery voltage only depends on the circuit parameters. Therefore, the value of  $u_c$  is constant under the same circuit parameters. The result shown in Figure 8 shows that when the time constant  $\tau$  is set to  $3 \times 10^{-5}$  s, the arc current and voltage change curves of the arc static voltage  $u_c$  are changed. It can be seen from Figure 8 that with the increase in  $u_c$ , the arcing voltage also increases accordingly, which is about 1.8 times that of  $u_c$ , and the time required for the arcing voltage to decrease to  $u_c$  increases, so the arc zero-crossing time gradually increases.

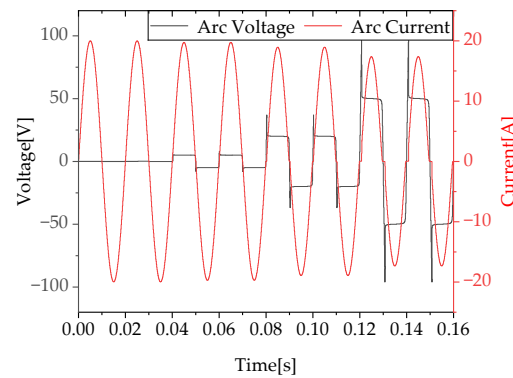


**Figure 8.** The arc voltage and current curves when  $u_c$  changes.

The arc time constant  $\tau$  reflects the internal physical process of the arc, and the static voltage of the arc depends more on the external circuit, so the arc time constant  $\tau$  can better highlight the mechanism of the random change of the arc current zero-crossing time. However, the existing arc model has not yet reflected this feature. Therefore, this paper proposed a model that reflects the random change of arc current zero-crossing time.

#### 4. Establishment of the Improved Arc Model

According to the random features of arc current at different stages of arc fault occurrence and development, the small signal analysis method was used to establish the model of the low-frequency component change trend and high-frequency component distribution law of the arc current, and then the two were superimposed to form the simulation model of arc fault electrical parameters.

##### 4.1. Low-Frequency Part

The Cassie model is appropriate for conditions characterized by low arc impedance at elevated current levels, whereas the Mayr model is appropriate for conditions with high arc impedance. The arc impedance is low during the occurrence of a series arc fault; therefore, this work used the enhanced Cassie model to simulate the arc associated with the series arc fault. According to the random features of arc current at different stages of arc fault occurrence and development, the small signal analysis method was used to establish the model of the low-frequency component change trend and high-frequency component distribution law of the arc current and then the two were superimposed to form the simulation model of arc fault electrical parameters.

Transforming (7) into

$$\tau = \left( \frac{u^2}{u_c^2} - 1 \right) / \left( \frac{d \ln g}{dt} \right) \tag{8}$$

Bring (5) into (8) to obtain

$$\tau = \frac{\frac{u^2}{u_c^2} - 1}{\frac{d \ln \left[ \left( \frac{V_m}{u} \sin \varphi - 1 \right) / r_0 \right]}{dt}} \tag{9}$$

That is,  $\tau$  changes with the breakdown phase angle  $\varphi$ .

Since the breakdown phase angle  $\varphi$  discussed in Section 3.1 changes according to the half-cycle, which affects the zero-crossing time, with it also changing according to the half-cycle, the time constant  $\tau$  can be inversely solved by the zero-crossing time distribution law of each half-cycle to reflect the randomness of the zero-crossing time distribution of the series arc current. From the analysis in Section 3.2, it can be seen that the arc current zero-crossing time satisfies the log-normal distribution and changes once every half-cycle.

Therefore, this paper calculates the change rate of arc current zero-crossing time in the half-cycle.

$$\frac{dt_0}{dt} = \frac{t_0(n) - t_0(n-1)}{T/2} \quad (10)$$

where  $t_0(n)$  and  $t_0(n-1)$  are the zero-crossing times corresponding to the  $n$ th half period and the  $(n-1)$ th half period, respectively. It can be seen from (5) that each  $t_0$  corresponds to a breakdown phase angle  $\varphi$ . Since the breakdown phase angle  $\varphi$  changes once every half-cycle, the average value of the arc voltage in the corresponding half-cycle is used instead of the instantaneous value of the arc voltage. The denominator part of (9) can be reduced to

$$\frac{d \ln \left[ \left( \frac{V_m}{u} \sin \varphi - 1 \right) / r_0 \right]}{dt} = \frac{\ln \left[ \frac{\frac{V_m}{U_{avg}(n)} \sin \varphi(n) - 1}{\frac{V_m}{U_{avg}(n-1)} \sin \varphi(n-1) - 1} \right]}{T/2} \quad (11)$$

where  $\varphi(n)$  and  $\varphi(n-1)$  denote the breakdown phase angles associated with the  $n$ -th half-cycle and the  $(n-1)$ -th half-cycle, respectively, and  $U_{avg}(n)$  and  $U_{avg}(n-1)$  are the average arc voltages for the  $n$ -th half-cycle and the  $(n-1)$ -th half-cycle, respectively. Consequently, the differential equation pertaining to the time constant of the arc model in (9) may be converted into a difference equation, which can be resolved by the iterative procedure.

The lognrnd function in MATLAB was applied to generate a log-normal distribution random number, which was substituted into (5) to calculate  $\varphi(n)$ , and then substituted into (11) to calculate  $\tau$ . Figure 9 shows the result of calculating the time constant of the arc current 500 times. It can be seen that the average value of  $\tau$  is  $1.43 \times 10^{-5}$  s, and most data points are concentrated below  $5 \times 10^{-5}$  s, which conforms to the law of arc current time constant  $\tau$  in Section 3.3.

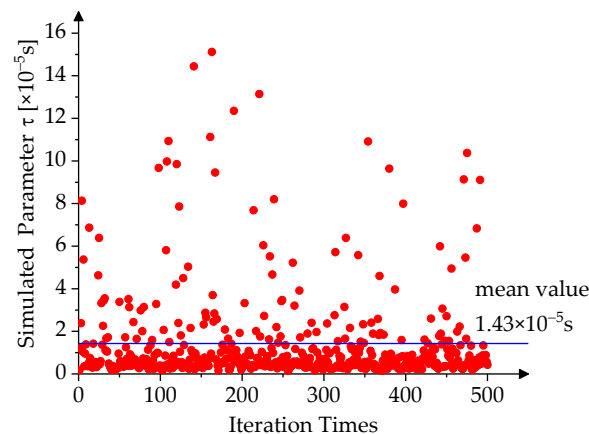


**Figure 9.** The arc current time constant simulation results.

#### 4.2. High-Frequency Part

When the arc fault occurs in the low-voltage distribution network system, more high-frequency noise will be generated in the bus current than during normal operation. In order to describe the features of the arc more completely, it is necessary to study the appropriate noise model and the arc time-domain model. At present, the commonly used noise models mainly include Gaussian white noise and various colored noise models. Although they can simulate the high-frequency features of the arc to a certain extent, they are not comprehensive. Therefore, the spectrum law under different current levels was analyzed.

It can be seen from Figure 4 that the arc current spectrum under different current levels has a similar trend in the frequency range above 1 kHz. In Figure 4, the arc current

spectrum amplitude of the solid line box part shows an overall decreasing trend with the increase in frequency, and the power spectral density of the pink noise also shows a decreasing process with the increase in frequency. Therefore, the spectrum of the red solid line box part can be simulated by pink noise. The current spectrum amplitude of the dotted box is basically unchanged, which is similar to the spectrum of Gaussian white noise. Therefore, this spectrum can be simulated by Gaussian white noise. From the above analysis, it can be seen that there is an approximate frequency segmentation point in the arc spectrum, and the arc spectrum has different change processes before and after the segmentation point. Therefore, the high-frequency component of the arc can be simulated by constructing the arc spectrum in segments. The equation is as follows:

$$S(f) = \begin{cases} \frac{l \times S_w(f)}{f^k} & f \leq f_0 \\ \frac{l \times S_w(f)}{f_0^k} & f \geq f_0 \end{cases} \quad (12)$$

In (12),  $S(f)$  is the spectrum amplitude of the improved noise model, and  $S_w(f)$  is the spectrum amplitude of the Gaussian white noise.  $f_0$  is the turning frequency point;  $l$  controls the amplitude of the spectrum; and  $k$  controls the rate at which the spectrum decreases with frequency before the turning frequency point.

The most important thing in the simulation model is the selection of parameters  $l$ ,  $f_0$ , and  $k$ . It is difficult to select the parameters artificially. Therefore, we selected the optimal values of the three parameters through the optimization algorithm. At present, there are many kinds of commonly used optimization algorithms, including particle swarm optimization, the firefly algorithm, the ant colony algorithm, the genetic algorithm, and so on. In this paper, the genetic algorithm was chosen to select the best parameters of the noise model. The main idea of the genetic algorithm is to learn from Darwin's evolutionary model under natural selection, simulate the problem to be solved into the process of biological evolution, encode the parameters to be solved into a chromosome, and generate the next generation of solutions through chromosome crossover and mutation operations. In addition, it is necessary to gradually eliminate the solution with a low fitness function value and increase the solution with a high fitness function value, so that after evolving  $N$  generations, a parameter with a high fitness function value is likely to evolve, that is, the optimization result of the objective function value. Table 4 shows the high-frequency part parameters of the arc current simulation model with different current levels.

**Table 4.** High-frequency part parameters of the arc current simulation model with different currents.

Current (A)	$L$	$k$	$f_0$
2.5	8.93	0.51	11,270.34
5	9.18	0.54	11,926.47
10	10.24	0.66	12,905.23
16	13.89	0.71	13,475.81
32	14.07	0.75	13,643.95

## 5. Discussion

### 5.1. Comparison and Analysis of the Distribution Features of Zero-Crossing Time

The actual arc current zero-crossing time was calculated as follows. The Phantom v611 high-speed camera was used to collect the arc image, and the openCV was used to detect the contour of the arc image and calculate the area of the arc bright spot. The arc bright spot area of 0 was regarded as the arc entering the zero-crossing period. The zero-crossing time of the simulated current of the arc model was compared with the zero-crossing time of the measured arc current, as shown in Figure 10.

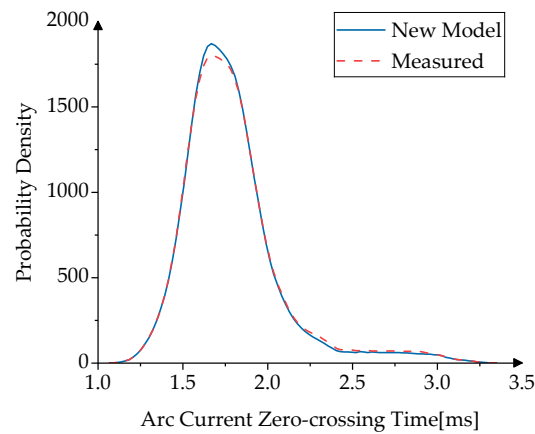


**Figure 10.** Comparison of the simulated and actual arc current zero-crossing time distributions.

It can be seen from Figure 10 that the simulation model can better reflect the distribution features of the arc current zero-crossing time. We confirmed the resemblance between the simulated and measured probability density waveforms of zero-crossing time by computing the Pearson correlation coefficient. The formula of the Pearson correlation coefficient is given as follows:

$$r = \frac{\sum (x_i - \bar{x})(y_i - \bar{y})}{\sqrt{\sum (x_i - \bar{x})^2 \sum (y_i - \bar{y})^2}} \quad (13)$$

In (13),  $x_i$  and  $y_i$  represent the data points for variables  $X$  and  $Y$ , respectively, while  $\bar{x}$  and  $\bar{y}$  denote the means of variables  $X$  and  $Y$ , respectively. The Pearson similarity between the simulation and the actual arc current zero-crossing time is 94.82%.

### 5.2. Verification of Time-Frequency Simulation Results of Arc Current

In order to verify the frequency domain performance of the arc fault current simulation model, the fast Fourier transform was performed on the simulated arc current and the measured arc current, respectively. The results are shown in Figure 11. The spectrum of the simulation data and the spectrum of the test part are basically the same, and the spectrum amplitude of the two is basically the same. The correlation coefficient between the calculated simulation and the measured current spectrum is 95.36%. On the whole, the simulation data can basically describe the typical frequency band of arc fault, which is of certain significance in analyzing the frequency domain features of arc fault.

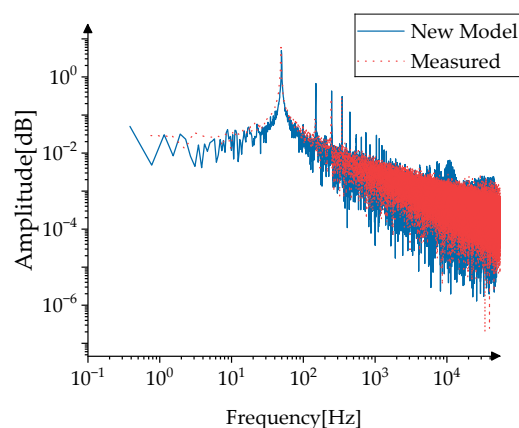


**Figure 11.** Comparison of the simulated and actual arc current spectrums.

According to the small signal analysis method, the low-frequency model was superimposed with the high-frequency model, and the simulation results with linear load are shown in Figure 12. The simulation current similarity is 99.16% and 99.73%, respectively.

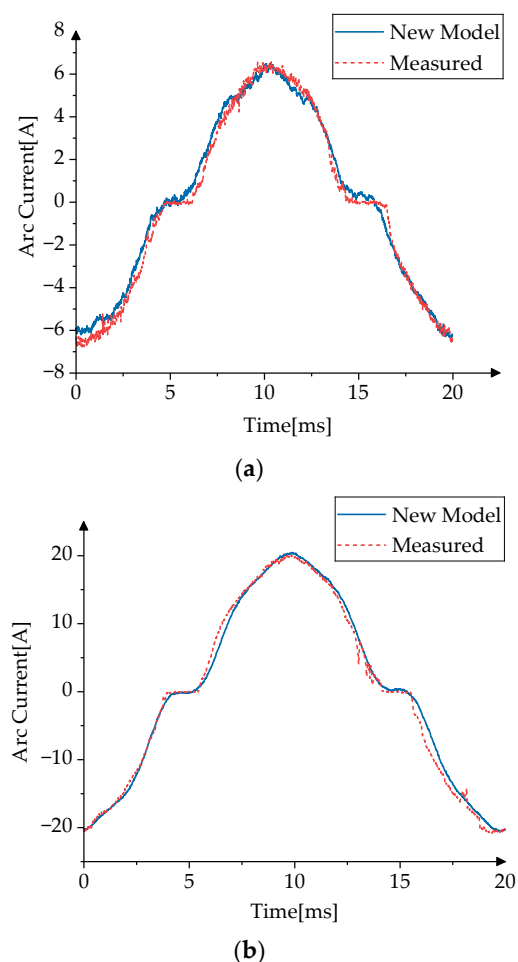


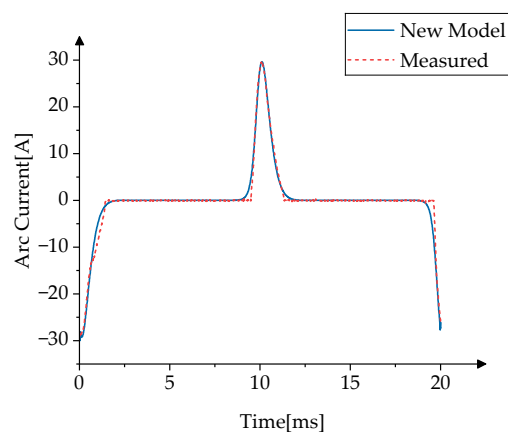
**Figure 12.** Comparison of the simulated and actual arc current waveforms with linear load. (a) Arc current waveforms of 5 A. (b) Arc current waveforms of 16 A.

The improved arc model was tested for both linear and nonlinear loads. Figure 13 illustrates a comparison between the predicted arc current waveform and the measured arc current waveform in the presence of nonlinear loads. The simulated current waveform exhibits a similarity of 99.03%, demonstrating that the model effectively represents the arc current features of both linear and nonlinear loads, thus fulfilling the requirements for low-voltage AC arc analysis and characterization in real-world conditions.

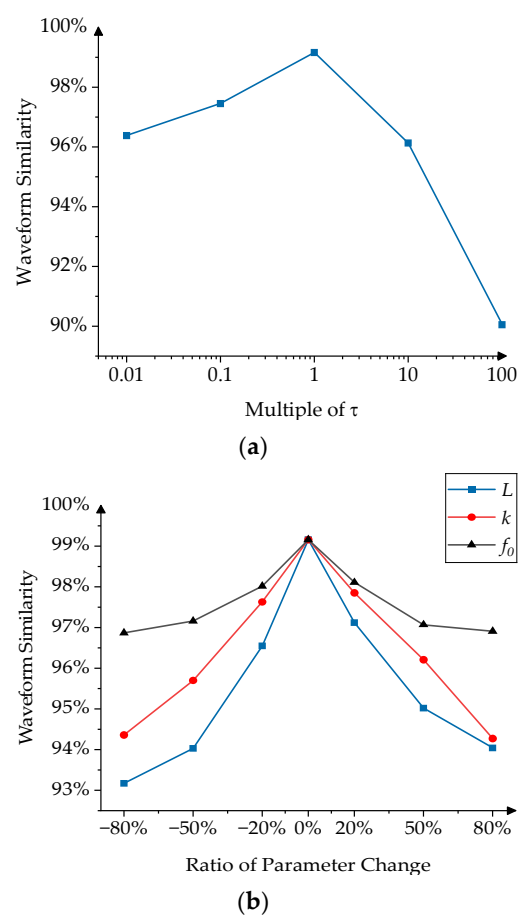
To ascertain which parameter exerts a more substantial influence on the model, we modified the mean of the arc time constant  $\tau$  and the parameters  $L$ ,  $k$ , and  $f_0$  of the piecewise noise model, based on the optimal parameters, to evaluate the effect of each parameter on model similarity. Figure 14 illustrates the outcome.

Figure 14a indicates that increasing  $\tau$  from the ideal matching value to 100 times significantly affects the resemblance between the arc current waveform produced by the model simulation and the measured arc current waveform. Nonetheless, when  $\tau$  is diminished to 0.01 times, the effect on waveform similarity is quite minimal. As examined in Section 3.3, when the value of  $\tau$  is really large, the arc voltage varies gradually, resulting in considerable distortion at the zero-crossing time. When  $\tau$  is minimal, the rate of change in arc voltage is rapid, and the zero-crossing time of arc current closely aligns with the optimal match;

however, jitter occurs at the zero-crossing point of the current. Nonetheless, this exerts a negligible influence on the current waveform during the entire cycle.



**Figure 13.** Comparison of the simulated and actual arc current waveforms with nonlinear load.



**Figure 14.** The influence of different parameters on model precision. (a) The influence of  $\tau$ . (b) The influence of the parameters of the high-frequency model.

In Figure 14b, the amplitude of medium-frequency and high-frequency signals generated by the high-frequency model of arc current is lower than that of low-frequency signals; thus, altering the parameters of the high-frequency model has minimal impact on its accuracy. The impact of the three parameters on the similarity between the simulated and measured arc current waveforms, from greatest to least, is as follows:  $L$ ,  $k$ ,  $f_0$ .



### 5.3. Comparison with Other Models

To validate the precision of the model presented in this paper, the original Cassie model, the Mayr model, the improved Mayr model [17], and the enhanced model with high frequency [20] were employed for waveform similarity assessment, as illustrated in Table 5.

**Table 5.** Comparison of the similarity of the simulated current waveforms of different arc models.

Arc Model	Randomness	High-Frequency Feature	Nonlinear Load	Waveform Similarity
Proposed model	Yes	Yes	Yes	99.16%
Improved Mayr model [17]	Yes	No	No	\
Enhanced Model with High Frequency [20]	No	Yes	No	\
Cassie model [26]	No	No	No	90.72%
Mayr model [26]	No	No	No	87.70%

The results shown in Table 5 indicate that the similarity of the current simulation waveform of the arc model, which accounts for the random and high-frequency features of the arc current zero-crossing time, is markedly superior to that of the conventional black box model. The randomness and high-frequency attributes of the arc current zero-crossing time are the principal features of arcs. This study presents a simulation model for arc fault electrical parameters that accounts for the stochastic nature of the zero-crossing time of an arc fault current and encompasses the high-frequency features of an arc fault current, thus providing a more precise representation of an actual arc fault current. Moreover, the proposed model's accuracy is validated against measured arc current data under both linear and nonlinear loads, demonstrating its applicability for low-voltage AC arcs in real-world conditions.

The arc model presented in this research effectively captures both the low-frequency random features and high-frequency traits of the arc current by enhancing the Cassie arc model. Arc fault detection methods typically rely on the detection of arc current features, with numerous detection techniques utilizing both low-frequency and high-frequency features of arc current through artificial intelligence (AI) models as presented in existing research. The advancement of AI methods for arc fault detection necessitates a substantial amount of data that precisely represent the features of arc current to train the arc detection network model. This paper presents an arc current simulation model capable of producing arc current data exhibiting both low- and high-frequency features, hence enhancing the training set for the arc detection network model and offering a foundational base for low-voltage AC series arc fault detection research.

## 6. Conclusions

In view of the fact that the existing models cannot reflect the high-frequency and random features of arc current, this paper proposed a mathematical model of arc current that combines the low-frequency randomness and high-frequency features of current. The accuracy of the model was verified by the actual collected arc current data, and the following conclusions were drawn:

(1) During the formation and development of the arc, the local electric field changes are caused by the electron collision caused by the field emission between the arcs, which leads to the random variation of the arcing voltage. The random variation of the arc current zero-crossing time reflects the random variation features of the arcing voltage. The mathematical statistics method was used to quantify the random distribution features of

the arc current zero-crossing time, and it was concluded that the arc current zero-crossing time conforms to the logarithmic normal distribution. By improving the Cassie arc time constant  $\tau$ , the randomness of the low-frequency signal of the arc current was accurately characterized.

(2) The frequency domain distribution of different arc currents has common features, which can be divided into three frequency bands: low, medium, and high. The low-frequency band features can be simulated by the Cassie model with improved time constant, and the piecewise noise model was established for the features of the medium-frequency band and the high-frequency band. The piecewise noise model uses the optimization algorithm to determine the model parameters, which solves the problem of deviation caused by empirical selection. The noise amplitude, change rate, and turning frequency control parameters are changed to enhance the flexibility and adaptability of the model.

(3) The segmented noise model was superimposed onto the low-frequency model of arc currents so that the entire arc simulation model could meet the distribution law of the arc current spectrum in the medium- and high-frequency bands in the frequency domain. At the same time, it can directly reflect the change of arc current zero-crossing time in the time domain, highlighting the random features of arc current.

The model presented in this study simultaneously captures the stochastic and high-frequency attributes of the arc, as validated under both linear and nonlinear loads, and holds considerable importance for understanding the features of low-voltage AC series arc current. This paper examines the factors influencing the zero-crossing time of arc current, beginning with the mechanism of arc formation, and proposes a research approach for periods when the zero-crossing features of arc current are not pronounced, such as during unstable or intermittent combustion, at the moment the arc initiates. Future studies may focus on the detection of latent arc faults in electrical lines, thereby addressing existing gaps in detection standards both domestically and internationally. With the development of artificial intelligence methods to detect arc fault technology, a large number of data that accurately reflect the features of arc current are needed to train the arc detection network model. The arc current simulation model established in this paper can generate arc current data with low-frequency and high-frequency features, which can optimize the training set of the arc detection network model and provide a corresponding research basis for low-voltage AC series arc fault detection.

**Author Contributions:** Conceptualization, Y.W. and Y.L.; methodology, Y.L. and D.S.; software, Y.L.; validation, Y.W., Y.L. and D.S.; formal analysis, Y.W. and Y.L.; investigation, Y.L. and T.L.; resources, Y.W. and X.N.; data curation, X.N.; writing—original draft preparation, Y.W., Y.L. and X.N.; writing—review and editing, Y.W. and Y.L.; visualization, Y.W., X.N. and D.S.; supervision, Y.W. and X.N.; project administration, Y.W.; funding acquisition, Y.W. All authors have read and agreed to the published version of the manuscript.

**Funding:** This research was funded by the Science and Technology Project of the State Grid Co., Ltd., grant number 5400-202326208A-1-1-ZN.

**Data Availability Statement:** Data are contained within the article. Data sharing is not applicable to this article.

**Conflicts of Interest:** The authors declare no conflicts of interest.

## References

1. There Have Been 660,000 Fire Accidents Across the Country in 2024. National Fire and Rescue Administration. 2024. Available online: [https://news.china.com.cn/2024-09/25/content\\_117448429.html](https://news.china.com.cn/2024-09/25/content_117448429.html) (accessed on 25 September 2024).
2. Fontana, C. Fractal Dimension Logarithmic Differences Method for Low Voltage Series Arc Fault Detection. In Proceedings of the 2021 5th International Conference on Smart Grid and Smart Cities (ICSGSC), Tokyo, Japan, 18–20 June 2021; pp. 77–81.

3. He, X.; Kawaguchi, T.; Hashimoto, S. Intelligent Identification Method of Low Voltage AC Series Arc Fault Based on Using Residual Model and Rime Optimization Algorithm. *Energies* **2024**, *17*, 4675. [[CrossRef](#)]
4. Su, S.; Xie, Q.; Ma, P.; Li, Y.; Chen, F.; Zhang, J.; Li, B.; Wang, C. A Single-Phase Ground Fault Line Selection Method in Active Distribution Networks Based on Transformer Grounding Mode Modification. *Energies* **2024**, *17*, 4743. [[CrossRef](#)]
5. Chen, S.; Wu, H.; Meng, Y.; Wang, Y.; Li, X.; Zhang, C. Reliable Detection Method of Variable Series Arc Fault in Building Integrated Photovoltaic Systems Based on Nonstationary Time Series Analysis. *IEEE Sens. J.* **2023**, *23*, 8654–8664. [[CrossRef](#)]
6. Qin, D.; Zhang, Z.; Zhang, D.; Xu, Y.; Wan, C.; Lakshmi, R.; Tohid, S.; Dong, D.; Cao, Y. Oscillation Issue and Solution for Solid-State Circuit Breaker Using High Power IGBT Module. *IEEE Trans. Ind. Applicat.* **2023**, *60*, 765–772. [[CrossRef](#)]
7. Dam, S.K.; Yang, C.-H.; Dong, Z.; Qin, D.; Chen, R.; Wang, F.; Bai, H.; Zhang, Z. Module Development for a High Specific Power Density High-Efficiency Cryogenic Solid-State Circuit Breaker for Electrified Aircraft Propulsion. *IEEE Trans. Power Electron.* **2024**, *39*, 13234–13247. [[CrossRef](#)]
8. Schavemaker, P.H.; Van Der Slui, L. An Improved Mayr-Type Arc Model Based on Current-Zero Measurements. *IEEE Trans. Power Deliv.* **2000**, *15*, 580–584. [[CrossRef](#)]
9. Wang, W.; Yan, X.; Li, X.; Guo, D.; Geng, Z. Investigation of the Arc Characteristics in a Nozzle with C<sub>4</sub>F<sub>7</sub>N/CO<sub>2</sub> Mixtures. *Energies* **2024**, *17*, 4593. [[CrossRef](#)]
10. Santos, D.F.N.; Lisnyak, M.; Almeida, N.A.; Benilova, L.G.; Benilov, M.S. Numerical Investigation of AC Arc Ignition on Cold Electrodes in Atmospheric-Pressure Argon. *J. Phys. D Appl. Phys.* **2021**, *54*, 195–202. [[CrossRef](#)]
11. Li, Y.; Zhang, R.; Yang, K.; Qi, Y. Research on an Equivalent Heat Source Model of the AC Arc in the Short Gap of a Copper-Core Cable and a Fire Risk Assessment Method. *Sensors* **2024**, *24*, 1443. [[CrossRef](#)] [[PubMed](#)]
12. Khakpour, A.; Franke, S.; Gortschakow, S.; Uhrlandt, D.; Methling, R.; Weltmann, K.-D. An Improved Arc Model Based on the Arc Diameter. *IEEE Trans. Power Deliv.* **2016**, *31*, 1335–1341. [[CrossRef](#)]
13. Ghavami, S.; Razi-Kazemi, A.A.; Niayesh, K. Estimation of the Arc Model Parameters Using Heuristic Optimization Methods. In Proceedings of the 2021 29th Iranian Conference on Electrical Engineering (ICEE), Tehran, Iran, 18–20 May 2021; IEEE: Piscataway, NJ, USA, 2021; pp. 296–301.
14. Gao, Y.; Wang, L.; Zhang, Y.; Zeng, K. Research on the Calculation Method for the Parameters of the Simplified Schavemaker AC Arc Model. In Proceedings of the 2018 Prognostics and System Health Management Conference (PHM-Chongqing), Chongqing, China, 26–28 October 2018; IEEE: Piscataway, NJ, USA, 2018; pp. 150–156.
15. Li, Q.; Xing, J.; Cong, H.; Chen, Q.; Li, J.; Chen, H. Arc simulation model considering the randomness of initial position of submerged arc. *High Volt. Eng.* **2015**, *41*, 1898–1906.
16. Wei, M.; Shi, F.; Zhang, H.; Jin, Z.; Terzija, V.; Zhou, J.; Bao, H. High Impedance Arc Fault Detection Based on the Harmonic Randomness and Waveform Distortion in the Distribution System. *IEEE Trans. Power Deliv.* **2020**, *35*, 837–850. [[CrossRef](#)]
17. Cui, J.; Sun, S.; Zhang, G.; Chen, Y.; Cui, B. Simulation method of ultra-fast transient overvoltage based on improved Mayr arc model of two-temperature magnetic fluid arc simulation. *Trans. China Electrotech. Soc.* **2024**, *39*, 5149–5161.
18. Zhao, H.; Liu, J.; Lou, J. Series Arc Fault Detection Based on Current Fluctuation and Zero-Current Features. *Electr. Power Syst. Res.* **2022**, *202*, 107–626. [[CrossRef](#)]
19. Li, L.; Li, Y.; Zhou, X.; Yang, Z.; Wang, K. Modeling of internal multiform intermittent arc fault for 10kV XLPE cable. *Trans. China Electrotech. Soc.* **2022**, *37*, 6104–6115.
20. Alabani, A.; Ranjan, P.; Jiang, J.; Chen, L.; Cotton, I.; Peesapati, V. Electrical Characterization and Modeling of High Frequency Arcs for Higher Voltage Aerospace Systems. *IEEE Trans. Transp. Electrific.* **2023**, *9*, 4716–4725. [[CrossRef](#)]
21. IEC 62606; General Requirements for Arc Fault Detection Devices. IEC: Geneva, Switzerland, 2017.
22. Zhou, T.; Yang, Q.; Yuan, T.; He, H.; Liu, H. A Novel Mathematical-Physical Arc Model and Its Application to the Simulation of High-Impedance Arc Faults in Distribution Networks. *IEEE Trans. Power Deliv.* **2024**, *39*, 1794–1806. [[CrossRef](#)]
23. Wang, W.; Li, J.; Lu, S. Application of Signal Denoising Technology Based on Improved Spectral Subtraction in Arc Fault Detection. *Electronics* **2023**, *12*, 3147. [[CrossRef](#)]
24. Xu, Z. *Fundamentals of Electrical Theory*, 1st ed.; Machinery Industry Press: Beijing, China, 2016; pp. 137–150.
25. Cao, Y. *Principles of Electrical Engineering*, 1st ed.; Machinery Industry Press: Beijing, China, 2016; pp. 143–145.
26. Liu, B.; Zeng, X. AC Series Arc Fault Modeling for Power Supply Systems Based on Electric-to-Thermal Energy Conversion. *IEEE Trans. Ind. Electron.* **2023**, *70*, 4167–4174. [[CrossRef](#)]

**Disclaimer/Publisher’s Note:** The statements, opinions and data contained in all publications are solely those of the individual author(s) and contributor(s) and not of MDPI and/or the editor(s). MDPI and/or the editor(s) disclaim responsibility for any injury to people or property resulting from any ideas, methods, instructions or products referred to in the content.